OPAL-PN281
28 February 1997

QCD studies with e^+e^- annihilation data at 172 GeV

The OPAL Collaboration

Abstract

As a continuation of the LEP 2 programme, we study hadronic events produced at a centre-of-mass energy of 172 GeV. We present distributions of event shape variables, jet rates, charged particle momentum spectra and multiplicities. We determine the strong coupling strength to be $\alpha_s(172\ \mathrm{GeV}) = 0.093 \pm 0.005(\mathrm{stat.}) \pm 0.006(\mathrm{syst.})$, the mean charged particle multiplicity to be $\langle n_{\mathrm{ch}}\rangle(172\ \mathrm{GeV}) = 25.92 \pm 0.56(\mathrm{stat.}) \pm 0.81(\mathrm{syst.})$ and the position of the peak in the $\xi_p = \ln(1/x_p)$ distribution to be $\xi_0(172\ \mathrm{GeV}) = 4.02 \pm 0.04(\mathrm{stat.}) \pm 0.02(\mathrm{syst.})$. Within the current statistical and systematic uncertainties, QCD Monte Carlo models and analytic calculations are in overall agreement with our measurements.

This note describes preliminary OPAL results to be submitted to the XVIII International Symposium on Lepton-Photon Interactions, Hamburg, 28 July - 1 August 1997, and to the International Europhysics Conference on High Energy Physics, Jerusalem, 19-26 August 1997

1 Introduction

In the second half of the 1996 running period, the LEP 2 programme advanced to produce e^+e^- annihilations at a centre-of-mass (c.m.) energy of $\sqrt{s} \approx 172$ GeV. We study the general features of hadronic decays of e^+e^- collisions at this energy as a continuation of our earlier publications at c.m. energies of $\sqrt{s} \approx 161$ GeV [1] and $\sqrt{s} = 130-136$ GeV [2].

Previous studies using e^+e^- annihilation data at c.m. energies up to $\sqrt{s} \approx 161$ GeV have shown that QCD based models and calculations give a good overall description of the observed data [1–7]. Here we examine the overall consistency of QCD at yet higher c.m. energies.

The majority of hadronic events produced at c.m. energies above the Z^0 resonance are 'radiative' events in which initial state photon radiation (ISR) reduces the energy of the hadronic system to about M_{Z^0}. An experimental separation between radiative and non-radiative events is therefore required. At energies above about 161 GeV, W^+W^- production becomes kinematically possible, and at 172 GeV the hadronic decays of the W bosons [8] contribute a significant background to the $(Z^0/\gamma)^*$ events.

In this paper we use the same techniques as in our previous analysis of e^+e^- annihilation data at c.m. energies of 161 GeV [1] and 130–136 GeV [2]. In section 2 we describe the samples of data and simulated events, in section 3 we explain our selection requirement and analysis procedures. In section 4 we present the event shape variables, jet rates, charged particle momentum spectra and multiplicities, and section 5 gives a summary and conclusion.

2 Data and Monte Carlo samples

The data sample used in this analysis, recorded with the OPAL detector [9], corresponds to an integrated luminosity of 10.42 ± 0.06 pb^{-1}. The mean c.m. energy of the sample is 172.1 GeV. All Monte Carlo event samples were generated at a c.m. energy of 171.0 GeV with full simulation of the OPAL detector [10].

Events for the process $e^+e^- \to (Z^0/\gamma)^* \to q\overline{q}$ will be referred to as '$(Z^0/\gamma)^*$ events'. We use a sample of 100 000 $(Z^0/\gamma)^*$ events generated using the PYTHIA 5.722 [11] parton shower Monte Carlo with initial and final state photon radiation and fragmentation of the parton final state handled by the routines of JETSET 7.408 [11]. As an alternative sample, we use 100 000 events generated with the HERWIG 5.9 [12] parton shower Monte Carlo. The Monte Carlo parameters have been tuned to OPAL data at the Z^0 -resonance [13][1].

In addition we generated events of the type $e^+e^- \to$ four-fermions (diagrams with quark and leptonic final states, including W^+W^- events, without intermediate gluons), using the grc4f 1.2 Monte Carlo model [14]. This generator is interfaced to JETSET 7.4 using the same parameter set for the parton shower, fragmentation and decays as described above for $(Z^0/\gamma)^*$ events. We employ in total 98 218 four-fermion events. For detailed studies of W^+W^- events, we use 40 000 events from PYTHIA.

[1]For comparison at the hadron-level we use version 5.9 of HERWIG with one parameter changed relative to our standard tuning [13], in order to improve the model's description of the mean charged particle multiplicity at the Z^0: Maximum cluster mass CLMAX = 3.75.

In addition to the Monte Carlo event generators discussed above, we use the QCD based event generators ARIADNE 4.08 [15] and COJETS 6.23 [16] in this study. All QCD models have shown to provide a good description of global e^+e^- event properties at $\sqrt{s} = M_{Z^0}$.

3 Analysis

3.1 Selection of events

In this note we use an extension of the selection criteria defined in [1]. We start with hadronic events, defined using the criteria as described in [17]. We define as particles both tracks recorded in the tracking chambers, with transverse momentum $p_T > 150$ MeV/c, and clusters recorded in the electromagnetic calorimeter, with a minimum energy of 100 MeV in the barrel and 250 MeV in the endcap sections [2]. To reject background from $e^+e^- \to \tau^+\tau^-$ and $\gamma\gamma \to q\overline{q}$ events and to ensure the events are well contained in the OPAL detector we require that

- the event has at least seven accepted tracks and
- the polar angle of the thrust axis lies within in the region $|\cos\theta_T| < 0.9$.

A total of 1 232 hadronic events pass these initial selection criteria.

To reject radiative events, we determine the effective c.m. energy of the observed hadronic system, $\sqrt{s'}$, as follows [18]. Isolated photons in the electromagnetic calorimeter are identified, and the remaining particles are formed into jets using the Durham [19] algorithm. The energy of additional photons emitted close to the beam directions is estimated by performing kinematic fits assuming zero, one or two such photons. The probabilities of the fits are used to select the most likely of these three scenarios. The value of $\sqrt{s'}$ is then computed from the fitted momenta of the jets, excluding photons identified in the detector or close to the beam directions. The value of $\sqrt{s'}$ is set to $\sqrt{s}$ if the fit assuming zero initial state photons was selected.

To reject events with large initial-state radiation, we require

- $\sqrt{s} - \sqrt{s'} < 10$ GeV.

This is referred to as the 'ISR fit' selection, which selects 273 non-radiative events. For systematic studies we use an alternative selection based on measurements of energy and momentum which we denote as the 'energy balance' [2]. In Figure 1a we compare the $\sqrt{s}-\sqrt{s'}$ distribution of the data to the $(Z^0/\gamma)^*$ and four-fermion events with full detector simulation[2]. The $(Z^0/\gamma)^*$ events are classified into strongly radiative events with $\sqrt{s} - \sqrt{s'_{\mathrm{true}}} > 10$ GeV (where $\sqrt{s'_{\mathrm{true}}}$ is the true effective c.m. energy, determined from Monte Carlo information), and non-radiative events, which is the complement. The contribution of W^+W^- events, simulated with PYTHIA, are indicated separately. Based on Monte

[2]To take into account the difference in c.m. energy between the data and Monte Carlo events, in Figure 1a we scaled $\sqrt{s}-\sqrt{s'}$ for Monte Carlo events by the ratio of c.m. energies of the data and Monte Carlo. This difference in c.m. energies has a negligible effect on the analysis.

Carlo studies we find that 19% of the events selected by the ISR fit are four-fermion events. The Monte Carlo predicts that about 93% of these four-fermion events originate from W^+W^- production.

The efficiency of the ISR fit selection to identify non-radiative $(Z^0/\gamma)^*$ events is 93%. The overall efficiency for the selection is 81%. Similar estimates of efficiencies and backgrounds are obtained if HERWIG is used instead of PYTHIA. The background from $e^+e^- \to \tau^+\tau^-$ and two-photon events of the type $\gamma\gamma \to q\overline{q}$ is estimated from Monte Carlo samples to be less than 0.3% and is consequently neglected.

The residual W^+W^- background is too large to be simply subtracted; we therefore first reduce it by applying a cut to remove W^+W^- events. As a cross check in our previous analysis [1] we used a cut on M_W^{fit} to reduce the background of W^+W^- events. The background rejection would be more effective if a cut on y_{34}^D were used, where y_{34}^D is the resolution parameter y_{cut}, in the Durham scheme, at which the event changes between three and four jets. However, it is not appropriate to cut on this variable in this analysis since we wish to study jet production rates. We found that instead, using a requirement on the QCD event weight W_{QCD} as described below, to reduce this background introduces a smaller bias.

We use a method to test the compatibility of the events with QCD-like production processes by computing the QCD event weight W_{QCD}. We consider the tree level, $\mathcal{O}(\alpha_s^2)$ [20], matrix element $|\mathcal{M}|^2$ for the processes $e^+e^- \to q\bar{q}q\bar{q}, q\bar{q}gg$, using the program EVENT2 [21]. Calculation of the event weight W_{QCD} proceeds by forcing the events to a four-jet configuration, using the Durham scheme:

$$W_{QCD} = \max_{\{p_1,p_2,p_3,p_4\}} \log\left(|\mathcal{M}(p_1,p_2,p_3,p_4)|^2\right) \tag{1}$$

with p_i the momenta of reconstructed jets. Since neither quark nor gluon identification is performed, we calculate the matrix element for each permutation of the jet-momenta and use the permutation with the largest value for the matrix element to define the event weight.

This 'quasi event-shape' is expected to have large values for processes described by the QCD matrix element, originating from $(Z^0/\gamma)^* \to q\overline{q}$, and smaller values for W^+W^- events. In Figure 1b we compare the data distribution of W_{QCD} to the expectations of our simulation. A clear separation between the $(Z^0/\gamma)^*$ and four-fermion events is achieved, by demanding

- $W_{QCD} \geq -0.5$.

After this requirement, the event sample consists of a total of 229 hadronic events. The four-fermion background is reduced from 19% to 7% whereas the total efficiency for non-radiative $(Z^0/\gamma)^*$ events is reduced from 81% to 78%. In Figure 2 we show, as an example, the effect of the four-fermion background rejection on the distribution of Thrust T (Figure 2a and 2b) and on y_{34}^D (Figure 2c and 2d). The background from W^+W^- events has predominantly low values for T, and is largely removed by our selection. The requirement on W_{QCD} has a small effect on y_{34}^D for $y_{34}^D < 0.01$, but reduces the y_{34}^D distribution for larger values.

3.2 Correction procedure

Bin-by-bin corrections are applied to the experimental distributions in a two stage process. In the first stage we correct for the presence of background from remaining four-fermion events by subtracting the expected background contribution. In the second stage, we use a bin-by-bin multiplication procedure to correct the observed distributions for the effects of detector resolution and acceptance as well as for the presence of radiative $(\mathrm{Z}^0/\gamma)^*$ events. For the multiplicity measurement presented in section 4.5, we use a matrix correction procedure to account for detector effects and radiative events rather than a bin-by-bin procedure.

For the bin-by-bin correction procedure, each bin of each observable is corrected from the 'detector-level' to the 'hadron-level' using two samples of Monte Carlo $(\mathrm{Z}^0/\gamma)^*$ events. The hadron-level does not include initial state radiation or detector effects and allows all particles with lifetimes shorter than 3×10^{-10} s to decay. The detector-level includes full simulation of the OPAL detector and initial state radiation and contains only those events which pass the same cuts as are applied to the data. The bin-by-bin correction factors are derived from the ratio of the distributions at the hadron-level to those at the detector-level.

3.3 Systematic uncertainty

The evaluation of systematic uncertainties is described in [1]. Briefly, the analysis was repeated with information from tracks only or from electromagnetic clusters only. The analysis was restricted to the barrel region of the detector, requiring the thrust axis of accepted events to lie within the range $|\cos\theta_T| < 0.7$. For track based quantities the variation of the observables when the cut on the point of closest approach of the track to the collision point in the plane transverse to the beam, d_0, was changed from 2 to 5 cm, is evaluated.

Uncertainties arising from the selection of non-radiative events are estimated by repeating the analysis using the energy balance selection. The uncertainties associated with the description and subtraction of the four-fermion events are estimated by changing the requirement on the QCD event weight W_{QCD}. The maximum difference with the nominal selection was determined when this cut was changed to $W_{\mathrm{QCD}} \geq -0.8$ and $W_{\mathrm{QCD}} \geq 0$, which changes the four-fermion background in the selected sample between 10% and 5% respectively. The difference in the results when we use simulated $(\mathrm{Z}^0/\gamma)^*$ events generated using HERWIG instead of PYTHIA is taken as the uncertainty in the modelling of the $(\mathrm{Z}^0/\gamma)^*$ events. A variation of 5% of the four-fermion cross section is found to have a negligible effect.

In order to estimate the statistical components of the systematic terms, we apply the following procedure. A set of 26 independent samples of simulated events, containing on average the same number of events as the data, is passed through the same standard and systematically changed analysis procedures as the data. For each systematic change of the analysis, the variances σ^2 of the differences between the results for this change and the standard results are determined. These variances are compared to the actual differences δ observed in the data when the analysis is changed. We define the systematic error to be $\sigma_{(\text{syst.})} = \sqrt{\delta^2 - \sigma^2}$ ($\delta > \sigma$) or $\sigma_{(\text{syst.})} = 0$ ($\delta \leq \sigma$), which reduces the possible overestimation of systematic errors. In order to reduce bin-to-bin fluctuations in the magnitudes of the systematic uncertainties, we average the relative uncertainty over three neighbouring bins of the measured distributions.

4 Results

4.1 Event shape observables

We study the event shape observables Thrust (T), Thrust Major and Minor (T_{major} and T_{minor}), Oblateness (O), Sphericity (S), Aplanarity (A), C-parameter (C), Heavy Jet Mass (M_H) and Total and Wide Jet Broadening (B_T and B_W), which are defined in reference [2] and references therein.

The data distributions for T, T_{major}, T_{minor}, O, S and A are shown in Figure 3 and for C, M_H, B_T and B_W are shown in Figure 4. The predictions of the PYTHIA, HERWIG, ARIADNE and COJETS Monte Carlo models are also shown. Within the uncertainties, the Monte Carlo predictions of all four models are seen to be in overall agreement with the data.

We also study the event shape observables by computing their mean $\langle x \rangle$, width σ, and skewness $\gamma = m_3/\sigma^3$, where $m_3 = \langle (x - \langle x \rangle)^3 \rangle$ for a generic distribution x. In Figure 5 the differences for mean, width and skewness between the Monte Carlo predictions and the data are shown. In general we find good agreement of the Monte Carlo predictions with the data. The Monte Carlo distributions describe the mean of the data well but are slightly narrower, and are less skewed than the data.

The mean value of the Thrust distribution is shown in Figure 6 together with data from lower energy measurements [1–5, 22] and the predictions for the energy evolution from PYTHIA, HERWIG, ARIADNE and COJETS. The predictions of all four Monte Carlo models are in good agreement with our measurement.

4.2 Jet production rates

We measure the jet production rates using two recombination jet finding algorithms, the JADE (E0) [23] and Durham (D) [19] schemes, and two variations of a cone jet algorithm [24], all of which are implemented as described in our previous publication and references therein [2].

As in previous analyses [1, 2, 25] we define y_{cut} as the resolution parameter in the recombination schemes. For the cone jet algorithm we replace the minimum cone energy, ε, by $\varepsilon' = \varepsilon \cdot E_{\text{vis}}/\sqrt{s}$, where E_{vis} is the sum of the energies of all particles used in the jet finding. In our studies the jet rates are computed at fixed $\varepsilon = 7$ GeV as R is varied or at fixed $R = 0.7$ radians as ε is varied.

Figure 7 shows the jet rates for the E0, Durham and cone schemes, versus their resolution parameters. There are strong bin to bin correlations. The data are compared with the predictions of PYTHIA, HERWIG, COJETS and ARIADNE. The Monte Carlo predictions show good general agreement with the data. The differential 2-jet rate D_2 for the Durham scheme, where $D_2 = (1/\sigma)\mathrm{d}\sigma/\mathrm{d}y_{23}^{\mathrm{D}}$ with y_{23}^{D} the value of y_{cut} where the event changes, in the Durham scheme, from two to three jets, is shown in Figure 4. The mean, width and skewness values for this distribution are shown in Figure 5. The D_2 distribution is well described by the Monte Carlo models.

In Figure 8 we show the 3-jet rate with the E0 scheme at $y_{\rm cut} = 0.08$ at a c.m. energy of 172 GeV, together with measurements at lower e^+e^- c.m. energies [2,4,26]. The curve is a fit of the $\mathcal{O}(\alpha_s^2)$ QCD prediction [27] for the evolution of R_3 with c.m. energy to the data from 22 GeV to 161 GeV [2,28] and to our measurement at 172 GeV. The fit, dominated by lower energy data, has a central value of $\alpha_s(M_{Z^0}) = 0.121$, with $\chi^2/\text{d.o.f.} = 1.0$, where the statistical error from the fit is negligible.

4.3 Determination of α_s

The determination of the strong coupling strength α_s(172 GeV) is based on fits of the QCD predictions to the corrected distributions for $1-T$, M_H, B_T, B_W and D_2, with the D_2 distribution defined using the Durham jet scheme, as described in [1,2,25]. The theoretical descriptions of these five observables are the most complete, allowing the use of combined $\mathcal{O}(\alpha_s^2)$+NLLA QCD calculations [31–33]. We follow the procedures described in these references as closely as possible in order to obtain results which we can compare directly to our previous analysis. In particular, we choose the so-called ln(R)-matching scheme, and fix the renormalisation scale parameter, $x_\mu \equiv \mu/\sqrt{s}$, to $x_\mu = 1$, where μ is the energy scale at which the theory is renormalised.

We find satisfactory fits for all five observables. The fit ranges are identical to those in our previous publication [1,2]. The results are given in Table 1 and in Figure 9. The statistical uncertainties are estimated from the variance of α_s values derived from fits to 80 independent sets of simulated events, each with about the same number of events as the data.

The hadronisation uncertainty is defined by adding in quadrature: the larger of the changes in α_s observed when varying the hadronisation parameters b and σ_Q by $\pm$ 1 standard deviation about their tuned values [13] in PYTHIA; the change observed when the parton virtuality cutoff parameter is altered from $Q_0 = 1.9$ GeV to $Q_0 = 4$ GeV in PYTHIA, corresponding to a change of the mean parton multiplicity from 7.0 to 4.8; the change observed when on the parton level only the u, d, s and c quarks are considered in order to estimate potential quark mass effects; and both differences with respect to the standard result when HERWIG or ARIADNE are used to account for the hadronization effects, rather than PYTHIA. For all observables the hadronisation uncertainties, given in Table 1, are relatively small compared to the statistical or experimental systematic errors.

We estimate the dependence of our fit results on the renormalisation scale x_μ as in references [2,25], by repeating the fits using $x_\mu = 0.5$ and $x_\mu = 2$. We find variations which are generally smaller than the statistical uncertainties and which are highly correlated between all observables. We treat the variation of the scale x_μ as an asymmetric uncertainty on α_s.

The total uncertainty for each individual observable is computed by adding in quadrature the statistical, the experimental, the hadronisation and the scale uncertainties. The total uncertainty on α_s(172 GeV) is typically around 10%.

We also derive a combined result for the strong coupling strength at 172 GeV using the weighted average procedure as described in reference [25]. The statistical uncertainty of the combined result is estimated using 80 independent samples of Monte Carlo events in the same manner as for the individual measurements. Our final result is

$$\alpha_s(172\ \mathrm{GeV}) = 0.093 \pm 0.005(\mathrm{stat.}) \pm 0.006(\mathrm{syst.}). \quad (2)$$

When evolved to the scale of M_{Z^0} this result leads to $\alpha_s(M_{\mathrm{Z}^0}) = 0.101 \pm 0.009$. For comparison, our measurements at the M_{Z^0} energy with a slightly larger set of observables based on $\mathcal{O}(\alpha_s^2)$+NLLA QCD calculations yielded $\alpha_s(M_{\mathrm{Z}^0}) = 0.120 \pm 0.006$ [25]. In order to compare average α_s values using exactly the same theoretical predictions and observables, we compute the weighted average from our present fits to $1-T$, M_H, B_T and B_W which yields the same numerical value for α_s. Our previous analysis at $\sqrt{s} = M_{\mathrm{Z}^0}$ gave $\alpha_s(M_{\mathrm{Z}^0}) = 0.116 \pm 0.006$ from fits of the same predictions to the same observables. Our present determination of α_s is consistent within two standard deviations with our measurement at $\sqrt{s} = M_{\mathrm{Z}^0}$.

In Figure 10 we show our measurement (2) together with other measurements of the strong coupling strength [29, 30], as a function of the energy scale Q. The curve shows the $\mathcal{O}(\alpha_s^3)$ prediction for $\alpha_s(Q)$ using $\alpha_s(M_{\mathrm{Z}^0}) = 0.118 \pm 0.006$ as given in reference [29]. Our measurement of $\alpha_s(172\ \mathrm{GeV})$ is consistent with the running of α_s required by QCD.

4.4 Charged particle momentum spectra

In Figure 11 we show the distributions of the track momentum components parallel, $p_\perp^{\mathrm{in}}$, and perpendicular, $p_\perp^{\mathrm{out}}$, to the event plane. This plane is defined by the eigenvectors of the momentum tensor associated with the two largest eigenvalues, as in reference [2]. We observe good agreement between the PYTHIA, HERWIG and ARIADNE models and the data for both $p_\perp$ distributions. The $p_\perp^{\mathrm{in}}$ distribution of COJETS is somewhat steeper than the data and the other models. COJETS also overestimates the intermediate region of the $p_\perp^{\mathrm{out}}$ distribution.

In Figure 12a we show the the distribution of rapidity, y, relative to the Thrust axis [2]. The predictions of the four models are shown in the Figure. In addition, we show in the same figure the expectation of the PYTHIA Monte Carlo, normalised to the multiplicity observed in the data (see section 4.5). The area under the curves is the mean charged multiplicity, which is different for the four Monte Carlo models and the data. The predictions from PYTHIA, HERWIG and ARIADNE compare reasonably well to the data once the different charged particle multiplicities in data and Monte Carlo are taken into account. The COJETS Monte Carlo overestimates the production of charged particles with low values of y and does not agree with the data even if the different charged multiplicity is considered.

The fragmentation function, $1/\sigma \cdot \mathrm{d}\sigma_{\mathrm{ch}}/\mathrm{d}x_p$, and the ξ_p distribution, $1/\sigma \cdot \mathrm{d}\sigma_{\mathrm{ch}}/\mathrm{d}\xi_p$, where $x_p = 2p/\sqrt{s}$, $\xi_p = \ln(1/x_p)$ and p is the measured track momentum, are shown in Figures 12 (b) and 13 (a) together with the Monte Carlo predictions. The spectrum of charged particles with large momentum fraction x_p is well described by all Monte Carlo models. The shape of the ξ_p distribution is also well described by PYTHIA, HERWIG and ARIADNE, in contrast to COJETS. The COJETS Monte Carlo predicts too many particles in the region of the peak and at large values of ξ_p, where low momentum particles contribute.

The NLLA QCD calculations [34] predict the shape to be a Gaussian with higher moments (skewed Gaussian). We fit a skewed Gaussian to the region close to the peak of the ξ_p distribution [1] and determine the position of the peak, ξ_0, to be

$$\xi_0(172 \text{ GeV}) = 4.02 \pm 0.04(\text{stat.}) \pm 0.02(\text{syst.}), \quad (3)$$

The systematic error is detailed in Table 2. In Figure 13 (b) we show our measurement of ξ_0 together with measurements taken at lower c.m. energies [1–3, 5, 35] and a fit with one free parameter of the NLLA prediction to the lower energy data up to and including $\sqrt{s}$ = 161 GeV. The NLLA calculations, extrapolated to $\sqrt{s}$ = 172 GeV, predict 3.97 ± 0.01, which is consistent with our measurement. As noted in our previous publications [1, 2], the fit is dominated by contributions from the data points with small errors at 29 and 35 GeV.

In the modified leading-log approximation (MLLA) [36] the ξ_p distribution is predicted in terms of two parameters, a QCD scale Λ and a normalisation factor $K(\sqrt{s})$. The values of $K(\sqrt{s})$ obtained in reference [37] are consistent with a linear c.m. energy variation. A fit of the MLLA prediction for the ξ_p distribution to OPAL data recorded at a c.m. energy of 91 GeV [37] determined Λ and $K(M_{Z^0})$. Figure 13 (a) shows the prediction of the MLLA at $\sqrt{s}$ = 172 GeV as a shaded band, using the result for Λ from reference [37]. The upper edge of the band corresponds to $K(172 \text{ GeV}) = K(M_{Z^0}) = 1.28$ whereas the lower edge corresponds to $K(172 \text{ GeV}) = 1.14$ (extrapolated from the values in reference [37] using the linear c.m. variation mentioned above). The description of the data around the peak is good for the extrapolated value of $K(172 \text{ GeV})$, considering that there are no free parameters.

4.5 Charged particle multiplicity

Finally, we measure the charged particle multiplicity distribution and derive several related quantities from it. In particular, we evaluate the mean charged multiplicity $\langle n_{\text{ch}} \rangle$, the dispersion D, the normalised second moment C_2 and the second binomial moment $\mathcal{R}_2$ [1].

The charged particle multiplicity distribution, corrected for experimental effects using an unfolding matrix, is shown in Figure 14 (a). The COJETS model predicts too many high multiplicity events and clearly disagrees with the data. The PYTHIA, HERWIG and ARIADNE models describe the data reasonably well.

We determine the mean value, the dispersion and the higher multiplicity moments to be:

$$\begin{aligned}
\langle n_{\text{ch}} \rangle(172 \text{ GeV}) &= 25.92 \pm 0.56(\text{stat.}) \pm 0.81(\text{syst.}), \quad (4)\\
D(172 \text{ GeV}) &= 8.05 \pm 0.55(\text{stat.}) \pm 0.77(\text{syst.}),\\
\langle n_{\text{ch}} \rangle / D(172 \text{ GeV}) &= 3.22 \pm 0.20(\text{stat.}) \pm 0.24(\text{syst.}),\\
C_2(172 \text{ GeV}) &= 1.096 \pm 0.012(\text{stat.}) \pm 0.013(\text{syst.}) \text{ and}\\
\mathcal{R}_2(172 \text{ GeV}) &= 1.058 \pm 0.012(\text{stat.}) \pm 0.014(\text{syst.}).
\end{aligned}$$

The systematic errors are detailed in Table 2.

Alternatively, the mean charged multiplicity is computed by integrating the corrected rapidity distribution, or the fragmentation function. Both the rapidity distribution and the fragmentation function give a result consistent with the one from the direct measurement presented in this section. For example, the result found by integrating the fragmentation function is $\langle n_{\mathrm{ch}}\rangle(172\ \mathrm{GeV}) = 25.48 \pm 0.56(\mathrm{stat.}) \pm 0.60(\mathrm{syst.})$.

We compare our results with data recorded at lower c.m. energies and with analytic QCD or Monte Carlo predictions. The dispersion and higher moments are consistent with measurements made at lower c.m. energies [1, 2, 38], and in agreement with the QCD Monte Carlo and analytic (where available) predictions. The predicted values of $\langle n_{\mathrm{ch}}\rangle(172\ \mathrm{GeV})$ from PYTHIA and ARIADNE are 26.6 and 26.5 respectively, while that from HERWIG is 26.3; COJETS predicts a value of 29.2, which differs by more than three standard deviations from our measurement. Figure 14 (b) shows our measurement of $\langle n_{\mathrm{ch}}\rangle$ as well as those obtained at energies from 12 to 172 GeV [2–4, 6, 39, 40]. The dash-dotted curve shows the NLLA QCD prediction [41] for the energy evolution of the charged particle multiplicity, with parameters fitted to all data points between 12 and 161 GeV. The NLLA calculation predicts a mean charged multiplicity at 172 GeV of 26.7 ± 0.3.

5 Summary and conclusions

In this paper we have presented measurements of the properties of hadronic events produced at LEP at a c.m. energy of 172 GeV. We have kept our analysis as close as possible to our previous ones to guarantee comparability of results.

We have determined the corrected distributions for event shape observables, for jet rates using different jet finding algorithms, for the charged particle multiplicity and for charged particle momentum spectra. As in our previous publications at lower c.m. energies [1,2], we conclude that the predictions of the PYTHIA, HERWIG and ARIADNE Monte Carlo models are found to be in general agreement with the measured distributions. The COJETS Monte Carlo model describes the event shape distributions well, but overestimates the production of soft charged particles in the rapidity, $\xi_p = \ln(1/x_p)$ and n_{ch} distributions.

From a fit of $\mathcal{O}(\alpha_s^2)$+NLLA QCD predictions to four event shape distributions and the differential two jet rate distribution, we have determined the strong coupling strength to be $\alpha_s(172\ \mathrm{GeV}) = 0.093 \pm 0.005(\mathrm{stat.}) \pm 0.006(\mathrm{syst.})$. If this measurement is evolved to the Z^0 peak it results in $\alpha_s(M_{\mathrm{Z}^0}) = 0.101 \pm 0.009$ which may be directly compared to our previous measurement of $\alpha_s(M_{\mathrm{Z}^0}) = 0.116 \pm 0.006$ using the same set of observables and $\mathcal{O}(\alpha_s^2)$+NLLA QCD predictions.

The ξ_p distribution has been found to be reasonably well described by QCD NLLA and MLLA calculations, and the position of the peak was measured to be $\xi_0(172\ \mathrm{GeV}) = 4.02 \pm 0.04(\mathrm{stat.}) \pm 0.02(\mathrm{syst.})$. This is in agreement with the expectation for the energy evolution given by QCD NLLA calculations.

The mean charged particle multiplicity has been determined to be $\langle n_{\mathrm{ch}}\rangle(172\ \mathrm{GeV}) = 25.92 \pm 0.56(\mathrm{stat.}) \pm 0.81(\mathrm{syst.})$, in agreement with the NLLA QCD predictions and the

PYTHIA, HERWIG and ARIADNE Monte Carlo predictions. We have also determined the dispersion and second multiplicity moments.

Our QCD studies provide a consistent analysis of hadronic events in e^+e^- collisions at LEP 2. All results can directly be compared to lower c.m. energies and to future higher c.m. energies. We look forward to the collection of a larger data sample and a higher c.m. energy in order to improve the precision of our measurements.

References

[1] OPAL Coll., G. Alexander et al.: CERN-PPE/97-015 (1997), Sub. to Z. Phys. C

[2] OPAL Coll., G. Alexander et al.: Z. Phys. C 72 (1996) 191

[3] ALEPH Coll., D. Buskulic et al.: CERN-PPE/96-043 (1996), Sub. to Z. Phys. C

[4] L3 Coll., M. Acciarri et al.: Phys. Lett. B 371 (1996) 137

[5] DELPHI Coll., P. Abreu et al.: CERN-PPE/96-130 (1996), Sub. to Z. Phys. C

[6] DELPHI Coll., P. Abreu et al.: Phys. Lett. B 372 (1996) 172

[7] S. Bethke and J.E. Pilcher: Annu. Rev. Nucl. Part. Sci. 42 (1992) 251

[8] OPAL Coll., K. Ackerstaff et al.: *Production of* $\mathrm{W^+W^-}$ *in* $\mathrm{e^+e^-}$ *collisions at* $\sqrt{s} = 172$ *GeV*, Physics Note 273 (1997)

[9] OPAL Coll., K. Ahmet et al.: Nucl. Instrum. Methods A 305 (1991) 275

[10] J. Allison et al.: Nucl. Instrum. Methods A 317 (1992) 47

[11] T. Sjöstrand: Comput. Phys. Commun. 82 (1994) 74

[12] G. Marchesini et al.: Comput. Phys. Commun. 67 (1992) 465

[13] OPAL Coll., G. Alexander et al.: Z. Phys. C 69 (1996) 543

[14] J. Fujimoto et al.: KEK-CP-046 (1996), to appear in Comput. Phys. Commun.

[15] L. Lönnblad: Comput. Phys. Commun. 71 (1992) 15

[16] R. Odorico, Comp. Phys. Comm. 72 (1992) 238.
P. Mazzanti and R. Odorico: Nucl. Phys. B 394 (1993) 267

[17] OPAL Coll., G. Alexander et al.: Z. Phys. C 52 (1991) 175

[18] D. R. Ward, *Separation of Non-radiative* $(\mathrm{Z}^0/\gamma)^*$ *events at LEP2*, OPAL TN394 (1996)

[19] S. Catani et al.: Nucl. Phys. B 269 (1991) 432

[20] R. K. Ellis, D. A. Ross and A. E. Terrano, Nucl. Phys. B 178 (1981) 421

[21] S.Catani and M.H.Seymour, CERN-TH/96-28.

[22] TASSO Coll., W. Braunschweig et al.: Z. Phys. C 47 (1990) 187
AMY Coll., Y. Li et al.: Phys. Rev. D 41 (1990) 2675
ALEPH Coll., D. Buskulic et al.: Z. Phys. C 55 (1992) 209
DELPHI Coll., D. Aarnio et al.: Phys. Lett. B 240 (1990) 271
L3 Coll., B. Adeva et al.: Z. Phys. C 55 (1992) 39

[23] JADE Coll., W. Bartel et al.: Z. Phys. C 33 (1986) 23

[24] OPAL Coll., R. Akers et al.: Z. Phys. C 63 (1994) 197

[25] OPAL Coll., P. D. Acton et al.: Z. Phys. C 59 (1993) 1

[26] JADE Coll., S. Bethke et al.: Phys. Lett. B 213 (1988) 235
JADE Coll., W. Bartel et al.: Z. Phys. C 33 (1986) 23
MARK II Coll., S. Bethke et al.: Z. Phys. C 43 (1989) 325
MARK II Coll., G. Abrams et al.: Phys. Rev. Lett. 63 (1989) 1558
TASSO Coll., W. Braunschweig et al.: Phys. Lett. B 214 (1988) 286
AMY Coll., I. Park et al.: Phys. Rev. Lett. 62 (1989) 1713
L3 Coll., B. Adeva et al.: Phys. Lett. B 248 (1990) 464
OPAL Coll., M. Akrawy et al.: Z. Phys. C 49 (1991) 375

[27] S. Bethke, Z. Kunszt, D.E. Soper and W.J. Stirling: Nucl. Phys. B 370 (1992) 310

[28] OPAL Coll., M. Z. Akrawy et al.: Phys. Lett. B 235 (1990) 389

[29] S. Bethke: PITHA 96/30 (1996), Talk presented at the QCD Euroconference 96, Montpellier, France, July 4-12 (1996)

[30] M. Schmelling, Talk presented at the International Conference on High Energy Physics, Warsaw, Poland, July 25-31 (1996)

[31] S. Catani, L. Trentadue, G. Turnock and B.R. Webber: Nucl. Phys. B 407 (1993) 3

[32] S. Catani, G. Turnock and B.R. Webber: Phys. Lett. B 295 (1992) 269

[33] G. Dissertori and M. Schmelling: Phys. Lett. B 361 (1995) 167

[34] C.P. Fong and B.R. Webber: Nucl. Phys. B 355 (1991) 54

[35] TASSO Coll., W. Braunschweig et al.: Z. Phys. C 47 (1990) 187
MARK II Coll., A. Petersen et al.: Phys. Rev. D 37 (1988) 1
TPC Coll., H. Aihara et al.: LBL-23727 (1988)
AMY Coll., Y. Li et al.: Phys. Rev. D 411 (1990) 2675
ALEPH Coll., D. Buskulic et al.: Z. Phys. C 55 (1992) 209
DELPHI Coll., P. Abreu et al.: Phys. Lett. B 275 (1992) 231
L3 Coll., B. Adeva et al.: Phys. Lett. B 229 (1991) 199

[36] V. A. Khoze, Yu. L. Dokshitzer and S. I. Troyan: Int. J. Mod. Phys. A 7 (1992) 1875

[37] OPAL Coll., M. Z. Akrawy et al.: Phys. Lett. B 247 (1990) 617

[38] M. Schmelling: Physica Scripta 51 (1995) 683

[39] OPAL Coll., R. Akers et al.: Z. Phys. C 68 (1995) 203

[40] JADE Coll., W. Bartel et al.: Z. Phys. C 20 (1983) 187
TASSO Coll., W. Braunschweig et al.: Z. Phys. C 45 (1989) 193
TPC Coll., H. Aihara et al.: Phys. Lett. B 134 (1987) 299
HRS Coll., M. Derrick et al.: Phys. Rev. D 34 (1986) 3304
AMY Coll., H. Zheng et al.: Phys. Rev. D 42 (1990) 737
MARK II Coll., G. Abrams et al.: Phys. Rev. Lett. 64 (1990) 1334
ALEPH Coll., D. Buskulic et al.: Z. Phys. C 69 (1995) 15
DELPHI Coll., P. Abreu et al.: Z. Phys. C 50 (1991) 185
L3 Coll., B. Adeva et al.: Z. Phys. C 55 (1992) 39

[41] B.R. Webber: Phys. Lett. B 143 (1984) 501

	$1-T$	M_H	B_T	B_W	D_2
$\alpha_s(172\text{ GeV})$	**0.094**	**0.0945**	**0.100**	**0.0894**	**0.088**
fit range	$0.05-0.3$	$0.17-0.45$	$0.075-0.25$	$0.05-0.2$	$0.0023-0.130$
χ^2/d.o.f.	13/5	1.4/4	1.7/5	5.1/4	12/6
Statistical error	±0.0081	±0.0083	±0.0066	±0.0054	±0.0061
tracks only	<0.0001	<0.0001	<0.0001	$+0.0020$	$+0.014$
cluster only	$+0.0034$	<0.0001	-0.0054	<0.0001	<0.0001
W_{QCD}	<0.0001	<0.0001	<0.0001	<0.0001	$+0.0011$
energy balance	$+0.0077$	$+0.0026$	$+0.0028$	$+0.0037$	$+0.011$
Experimental syst.	±0.0084	±0.0026	±0.0061	±0.0042	±0.018
$b+1$ s.d.	$+0.0001$	$+0.0001$	$+0.0002$	$+0.0001$	-0.0001
$b-1$ s.d.	-0.0001	-0.0002	-0.0003	<0.0001	$+0.0001$
σ_q+1 s.d.	-0.0004	<0.0001	-0.0003	-0.0001	$+0.0001$
σ_q-1 s.d.	$+0.0004$	$+0.0001$	$+0.0002$	$+0.0001$	$+0.0001$
$Q_0=4$ GeV	-0.0006	$+0.0011$	-0.0010	$+0.0005$	$+0.0018$
udsc only	$+0.0008$	$+0.0002$	$+0.0016$	$+0.0010$	$+0.0020$
HERWIG 5.9	-0.0005	$+0.0005$	-0.0019	-0.0001	-0.0011
ARIADNE 4.08	$+0.0016$	$+0.0008$	$+0.0004$	$+0.0009$	$+0.0005$
Total hadronisation	±0.0020	±0.0015	±0.0027	±0.0014	±0.0030
$x_\mu=0.5$	-0.0025	-0.0018	-0.0039	-0.0018	-0.0005
$x_\mu=2$	$+0.0032$	$+0.0026$	$+0.0047$	$+0.0025$	$+0.0014$
Total error	$\pm$**0.012**	$\pm$**0.0091**	$\pm$**0.010**	$\pm$**0.0073**	$\pm$**0.019**

Table 1: Values of $\alpha_s(172\text{ GeV})$ derived using the $\mathcal{O}(\alpha_s^2)$+NLLA QCD calculations with $x_\mu=1$ and the $\ln(R)$-matching scheme, fit ranges and χ^2/d.o.f. values for each of the five event shape observables. In addition the statistical and systematic errors are given. Where a signed value is quoted, this indicates the direction in which $\alpha_s(172\text{ GeV})$ changed with respect to the default analysis.

	ξ_0	$\langle n_{\mathrm{ch}} \rangle$		D	$\langle n_{\mathrm{ch}} \rangle / D$	C_2	$\mathcal{R}_2$
		frag.	mult.				
standard result	4.02	25.48	25.92	8.05	3.22	1.096	1.058
statistical error	0.04	0.56	0.56	0.55	0.20	0.012	0.012
energy balance	+0.01	+0.37	−0.32	<0.01	<0.01	<0.001	<0.001
$\|d_0\| < 5$ cm	<0.01	+0.18	+0.32	+0.28	−0.07	+0.004	+0.004
$\|\cos\theta_T\| < 0.7$	<0.01	<0.01	<0.01	<0.01	<0.01	<0.001	<0.001
W_{QCD}	+0.01	+0.22	+0.65	+0.70	−0.23	+0.012	+0.013
HERWIG	+0.01	-0.35	+0.16	+0.13	−0.03	+0.001	+0.002
Tot. syst. error	0.02	0.60	0.81	0.77	0.24	0.013	0.014

Table 2: Results with statistical and systematic uncertainties for the position ξ_0 of the peak of the ξ_p distribution, for $\langle n_{\mathrm{ch}} \rangle$ based upon measurements of the multiplicity distribution (mult.) or the fragmentation function (frag.), the dispersion D, the ratio $\langle n_{\mathrm{ch}} \rangle / D$ and the second moments C_2 and $\mathcal{R}_2$. The signs indicate the direction of the changes with respect to the standard analysis.

Figures

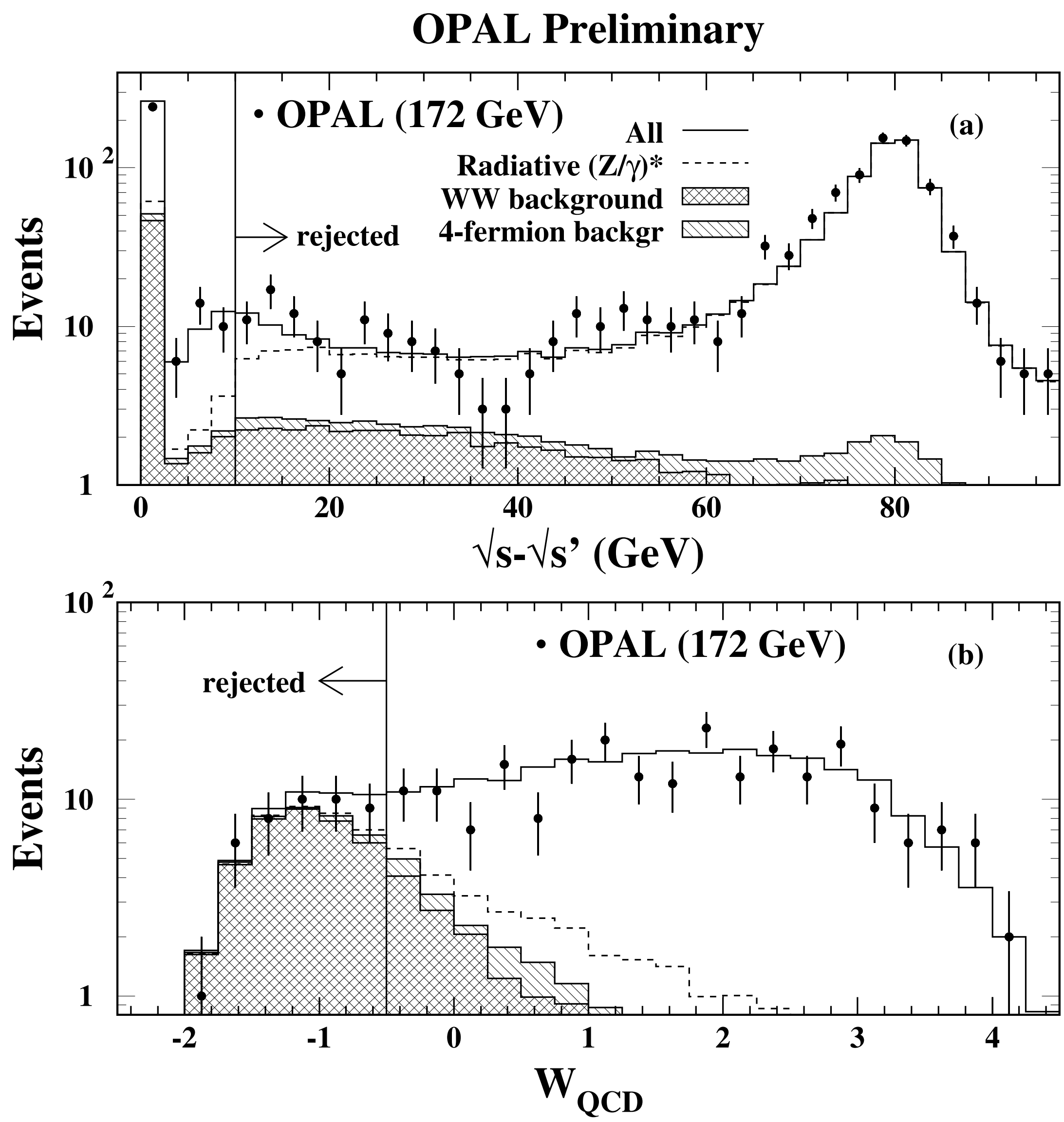

Figure 1: (a) Distribution of $\sqrt{s}-\sqrt{s'}$ for the data (full points) compared to Monte Carlo predictions. The cross-hatched histogram indicates the background from the W^+W^- events, predicted by PYTHIA. The left-hatched histogram corresponds to the total estimated four-fermion background, including the W^+W^- events, as predicted by the grc4f Monte Carlo. The full line corresponds to the total Monte Carlo prediction, including the full $(Z^0/\gamma)^*$ sample. The radiative background is indicated by the dashed line. The distributions of $\sqrt{s}-\sqrt{s'}$ of the Monte Carlo events is scaled to take into account the difference in c.m. energies between the data (172.1 GeV) and Monte Carlo (171 GeV). (b) The QCD event weight W_{QCD} for events that survive the requirement $\sqrt{s}-\sqrt{s'} < 10$ GeV.

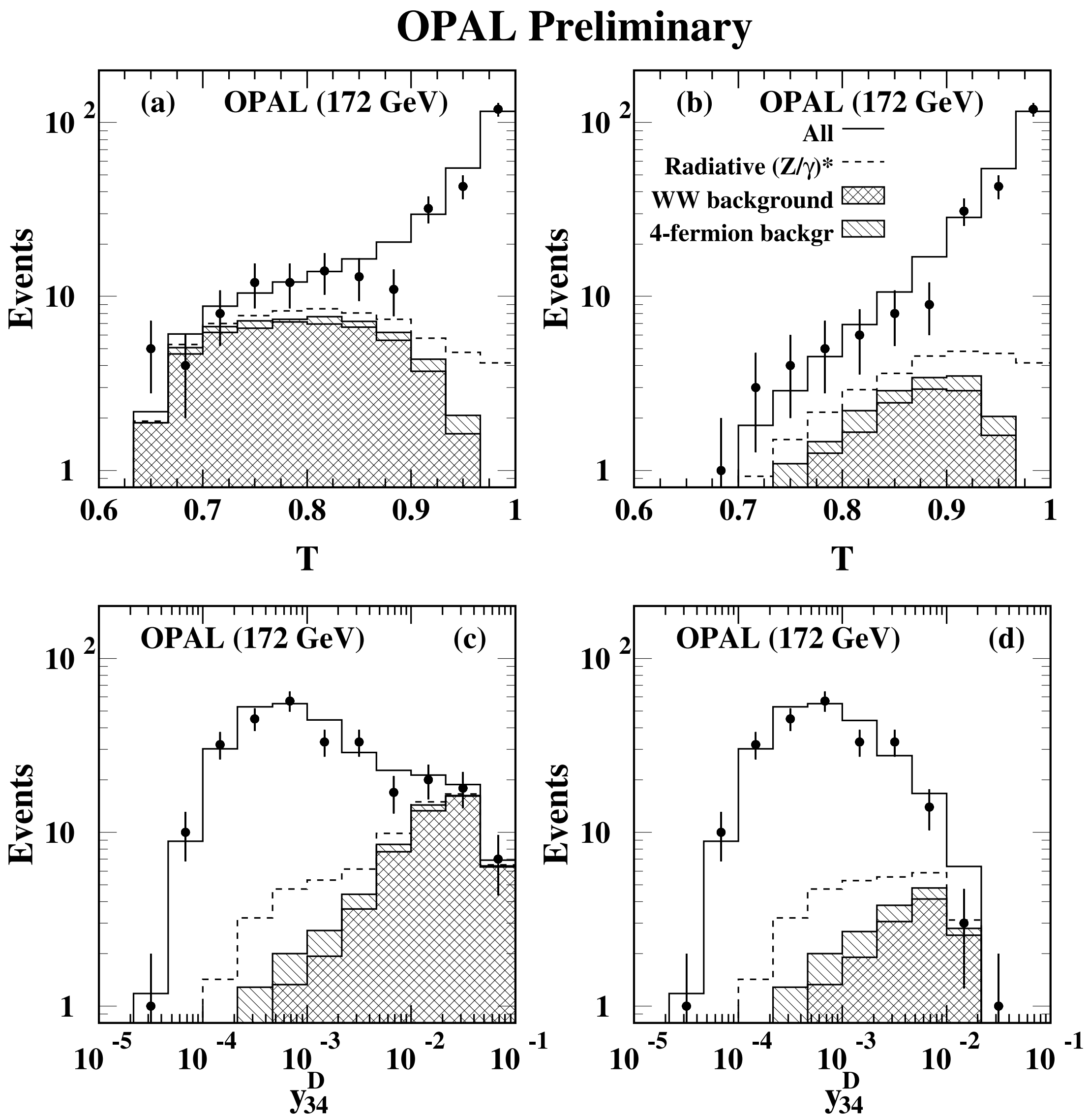

Figure 2: (a) The distribution for Thrust T without the requirement on the QCD event weight $W_{\rm QCD}$. The cross-hatched histogram indicates the background from the W^+W^- events, predicted by PYTHIA. The left-hatched histogram corresponds to the total estimated four-fermion background, including the W^+W^- events, as predicted by the grc4f Monte Carlo. The full line corresponds to the total Monte Carlo prediction, including the full $(Z^0/\gamma)^*$ sample. The radiative background is indicated by the dashed line. (b) The same quantity, after the requirement $W_{\rm QCD} \geq -0.5$. (c) The resolution variable $y_{\rm cut}$ for which the number of resolved jets in the event changes, according to the Durham scheme, from three to four jets, $y_{34}^{\rm D}$. No selection cut on the QCD event weight $W_{\rm QCD}$ is made. (d) The same quantity, but the requirement $W_{\rm QCD} \geq -0.5$ is imposed.

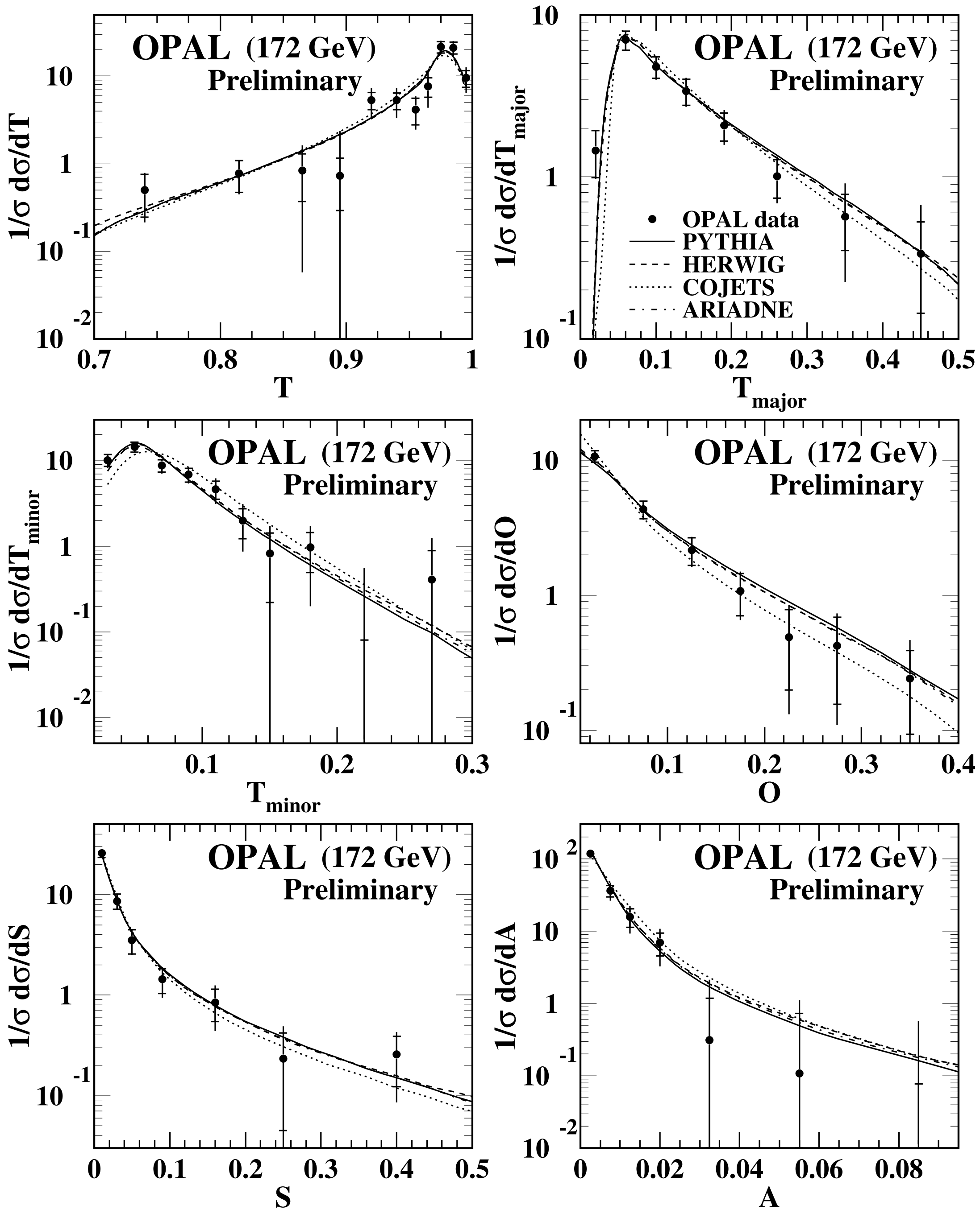

Figure 3: Distributions of the event shape observables Thrust T, Thrust Major T_{major}, Thrust Minor T_{minor}, Oblateness O, Sphericity S and Aplanarity A. Experimental statistical errors are delimited by the small horizontal bars. The total errors are shown by the vertical error lines. Hadron level predictions from PYTHIA, HERWIG, COJETS and ARIADNE are also shown. Points not on the plots have negative central values after background subtraction.

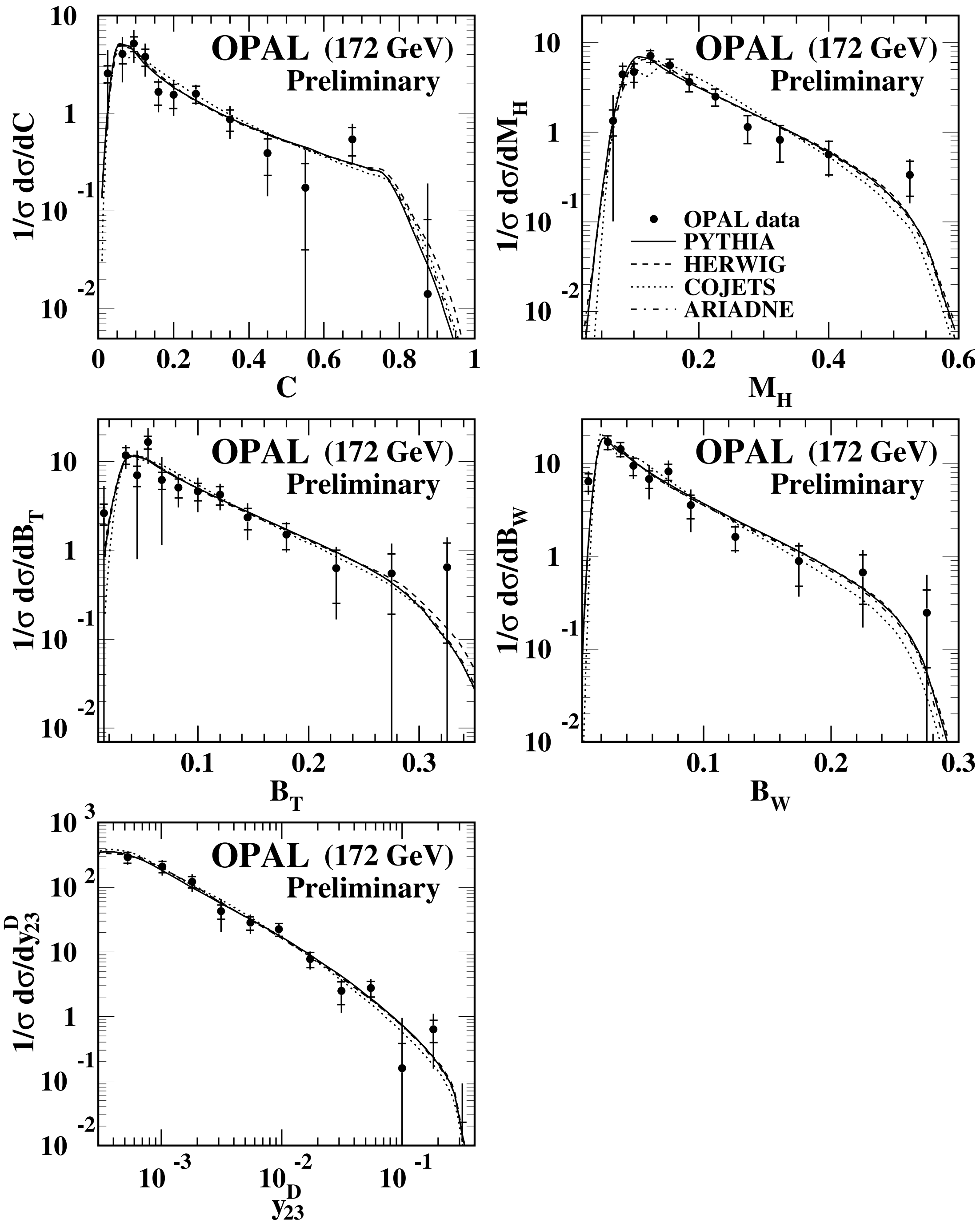

Figure 4: Distributions of the event shape observables C-parameter C, Heavy Jet Mass M_H, Total Jet Broadening B_T, Wide Jet Broadening B_W, and the Differential 2-jet rate D_2 using the Durham scheme. Experimental statistical errors are delimited by the small horizontal bars. The total errors are shown by the vertical error lines. Hadron level predictions from PYTHIA, HERWIG, COJETS and ARIADNE are also shown.

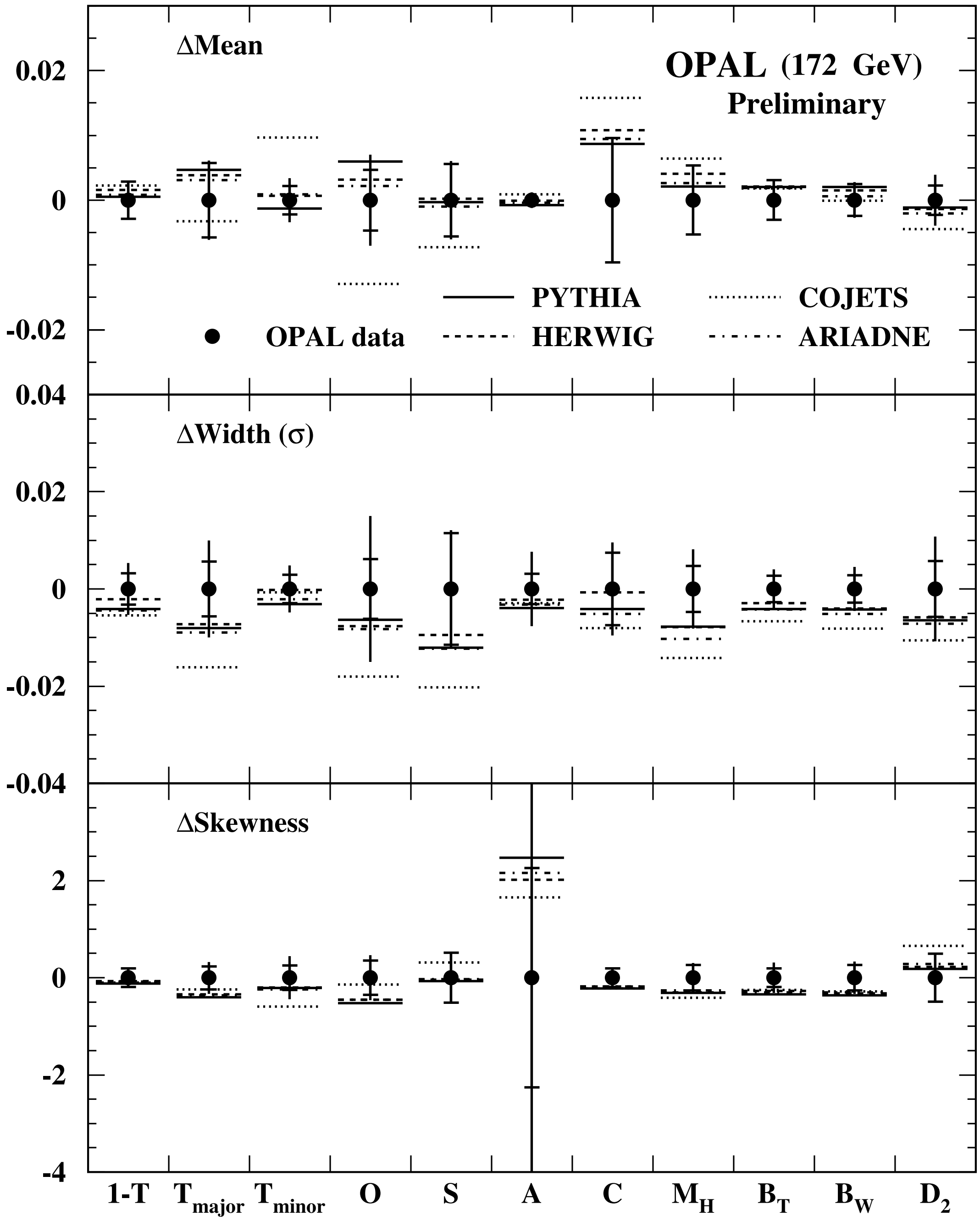

Figure 5: Difference of the PYTHIA, HERWIG, COJETS and ARIADNE predictions relative to the data (shown as full points with error bars) for the mean, width and skewness of event shape distributions.

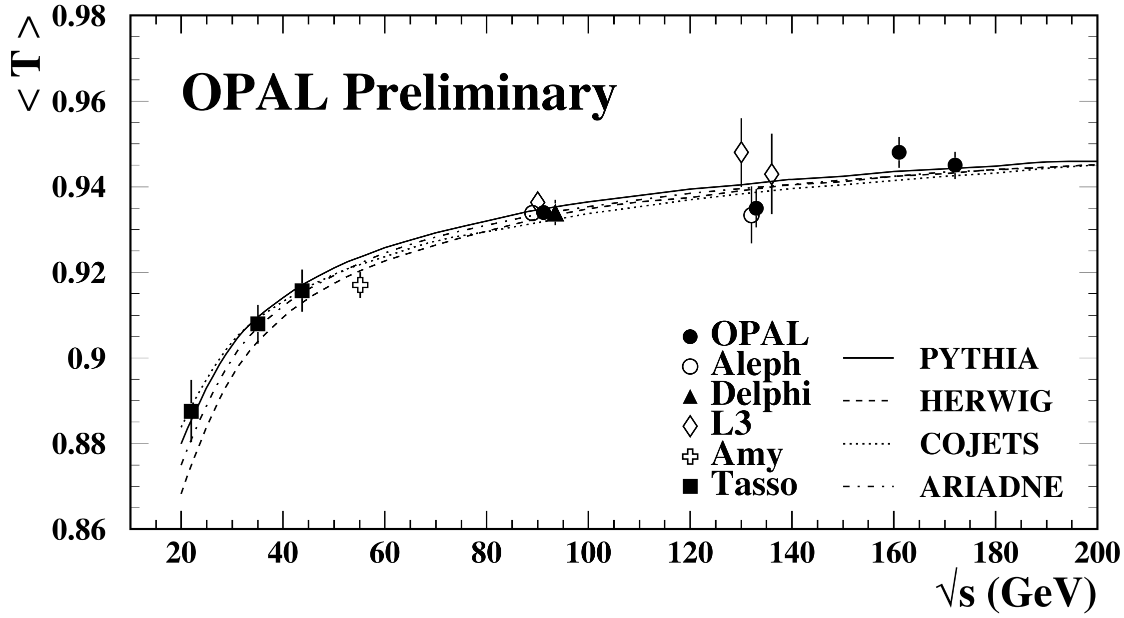

Figure 6: The mean Thrust value as a function of $\sqrt{s}$ from 22 GeV to 172 GeV. The measurements are compared to the predictions of PYTHIA, HERWIG, ARIADNE and COJETS.

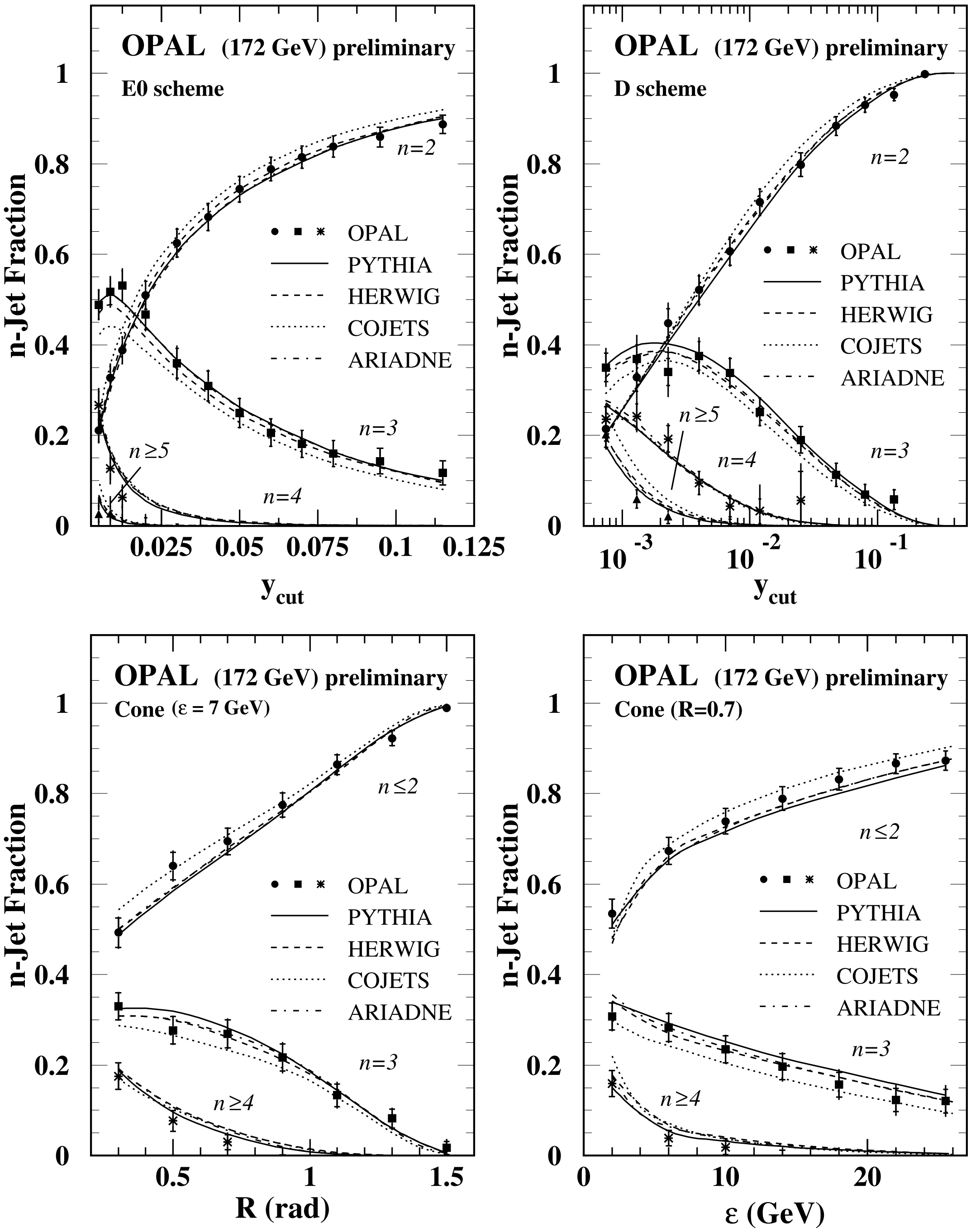

Figure 7: The fraction of the 2-, 3-, 4- and 5- or more jet events as a function of $y_{\rm cut}$ for the JADE (E0) and Durham (D) jet finding schemes, and the fraction of 2-, 3- and 4- or more jet events as a function of the energy cutoff ε or the cone half angle R for the cone jet finder. Hadron level predictions from PYTHIA, HERWIG, COJETS and ARIADNE are also shown.

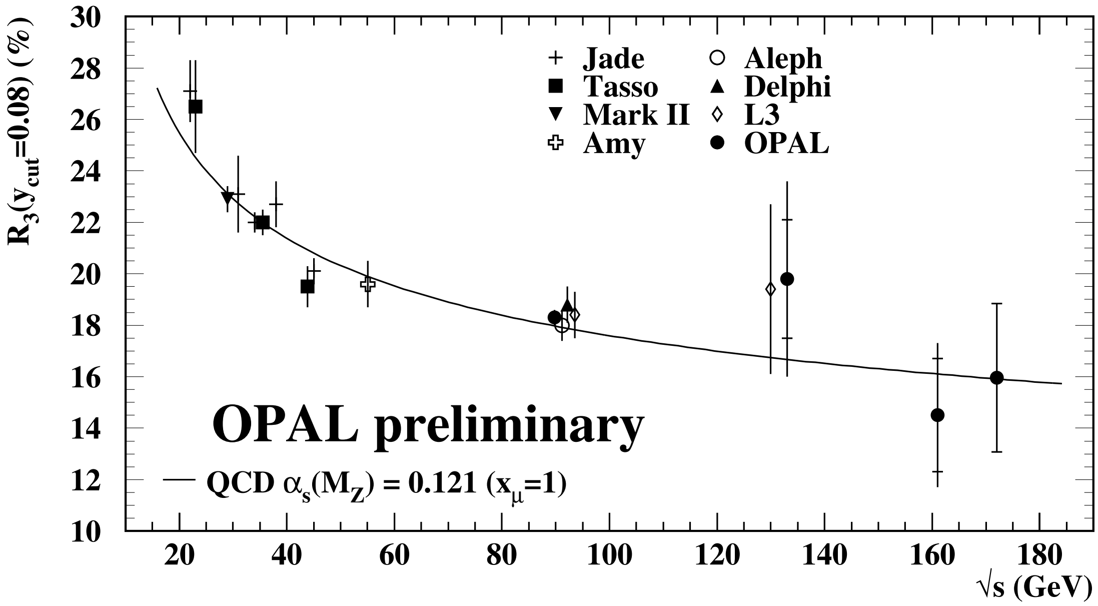

Figure 8: The three-jet rate (R_3) at $y_{\rm cut} = 0.08$ for the JADE (E0) jet finder, for values of $\sqrt{s}$ between 22 GeV and 172 GeV. The result of a fit of the $\mathcal{O}(\alpha_s^2)$ QCD prediction to the data is also shown.

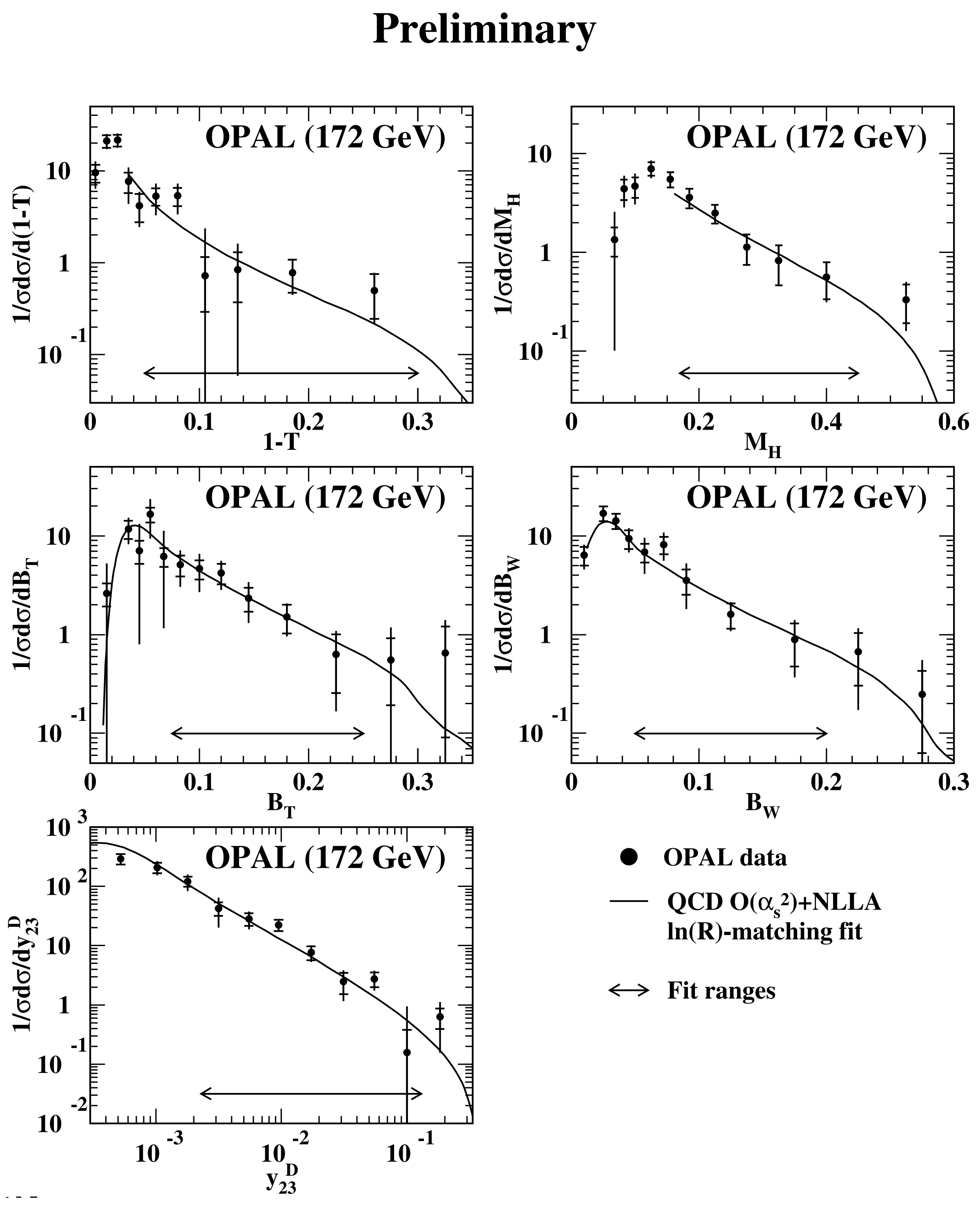

Figure 9: Distributions of the event shape observables Thrust $1-T$, Heavy Jet Mass M_H, Total B_T and Wide B_W Jet Broadening, and the Differential 2-jet rate D_2 using the Durham scheme are shown together with fits of the $\mathcal{O}(\alpha_s^2)$+NLLA QCD predictions. The fitted regions are indicated by the arrows.

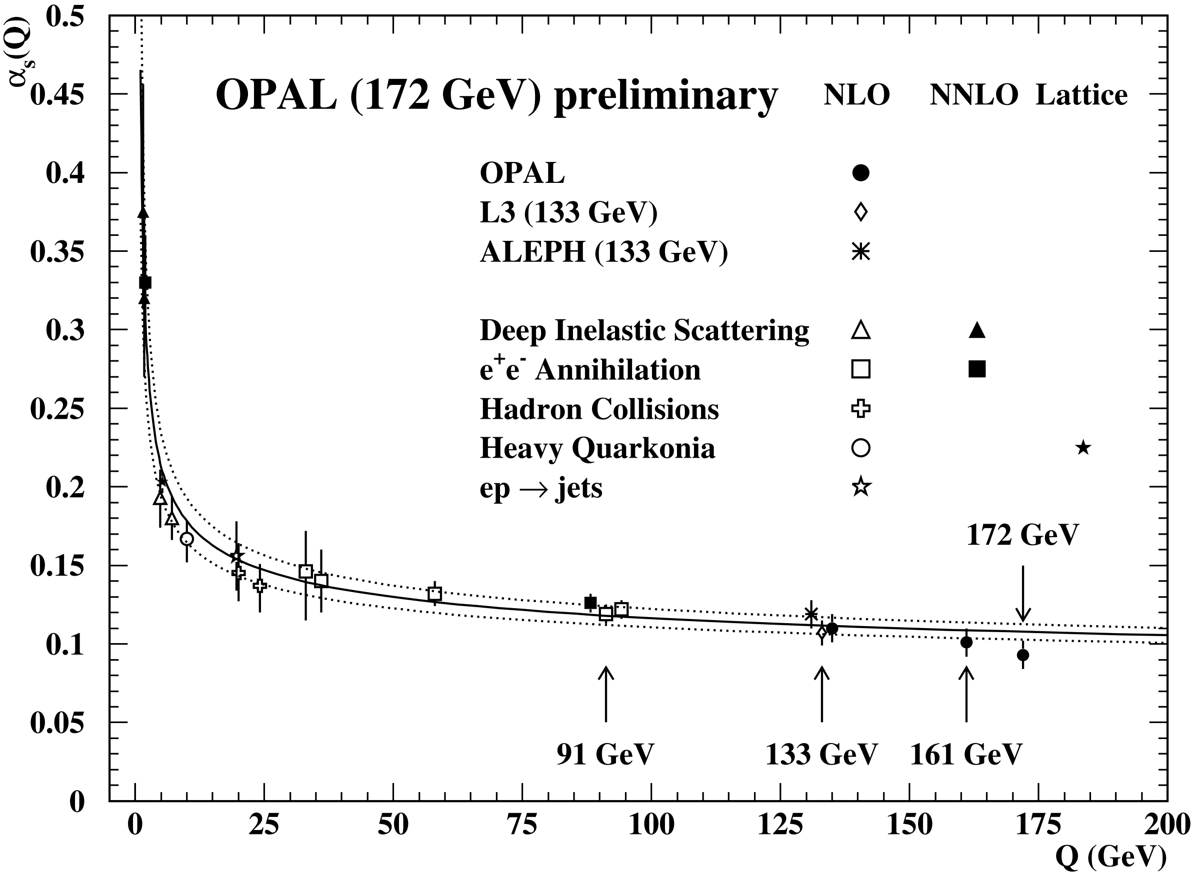

Figure 10: Values of α_s as function of energy [29]. The labels NLO and NNLO refer to the order of calculation used. NLO corresponds to $\mathcal{O}(\alpha_s^2)$ in e^+e^- annihilations, and NNLO to $\mathcal{O}(\alpha_s^3)$. The label Lattice refers to α_s values determined from lattice QCD calculations. The curves show the $\mathcal{O}(\alpha_s^3)$ QCD prediction for $\alpha_s(Q)$ using $\alpha_s(M_{Z^0}) = 0.118 \pm 0.006$; the full line shows the central value while the dotted lines indicate the variation given by the uncertainty.

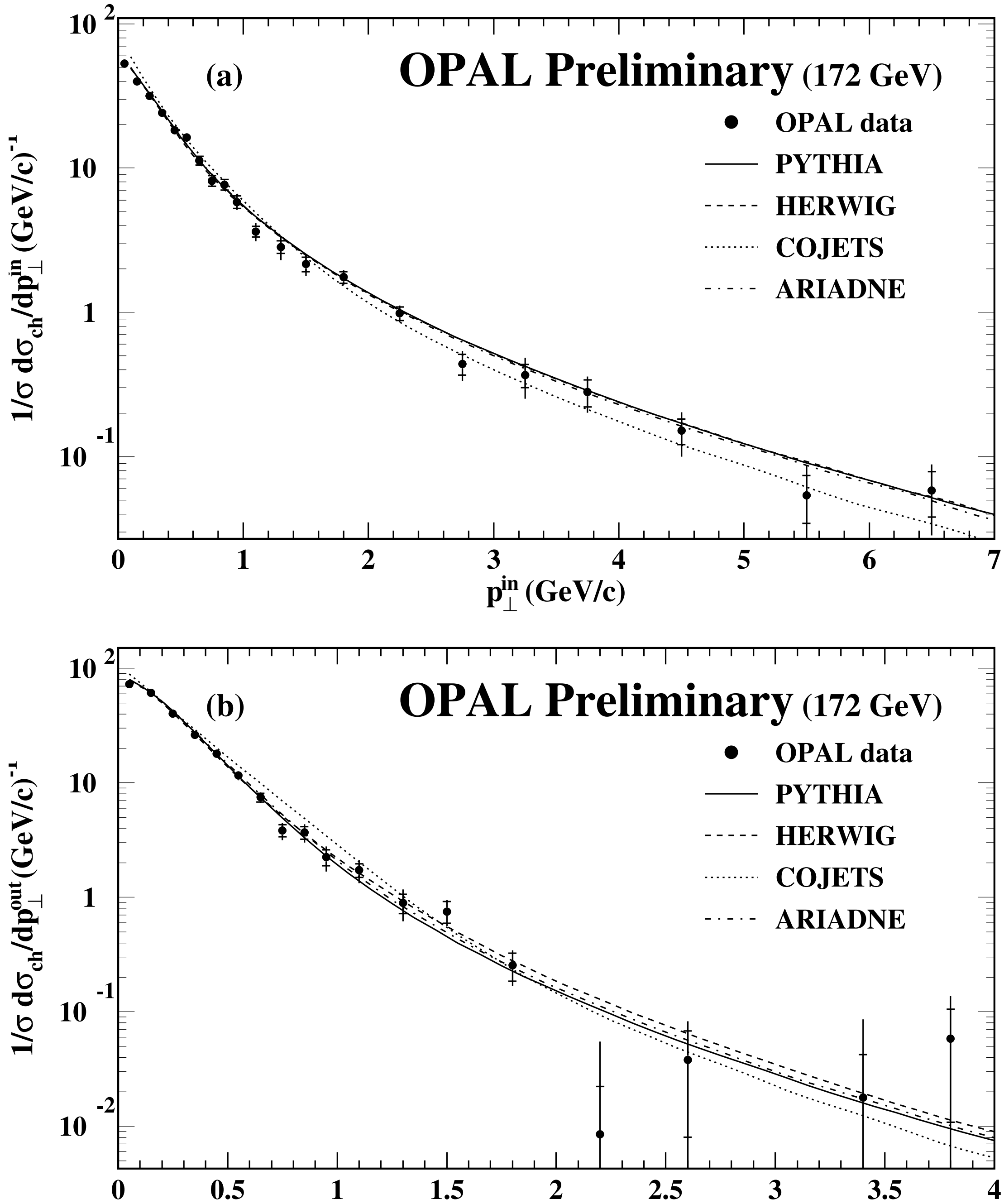

Figure 11: Distributions of momentum spectra in, $p_\perp^{\rm in}$, and out, $p_\perp^{\rm out}$, of the event plane for charged particles, compared to PYTHIA, HERWIG, COJETS and ARIADNE.

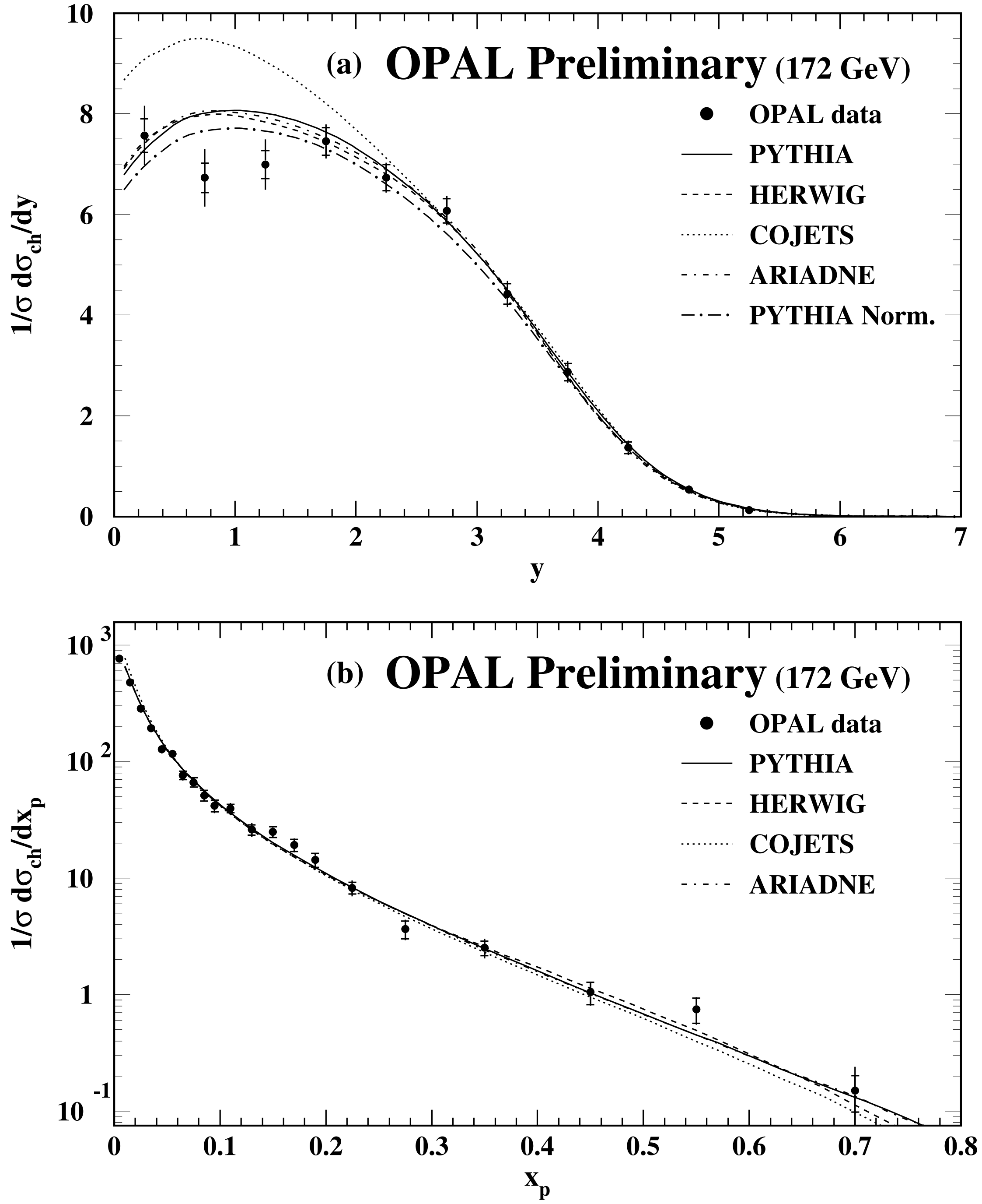

Figure 12: Distribution of Rapidity, y, and the fragmentation function for charged particles, compared to PYTHIA, HERWIG, COJETS and ARIADNE predictions. In Figure (a) we also show the prediction of the PYTHIA Monte Carlo, normalised to the charged multiplicity observed in the data.

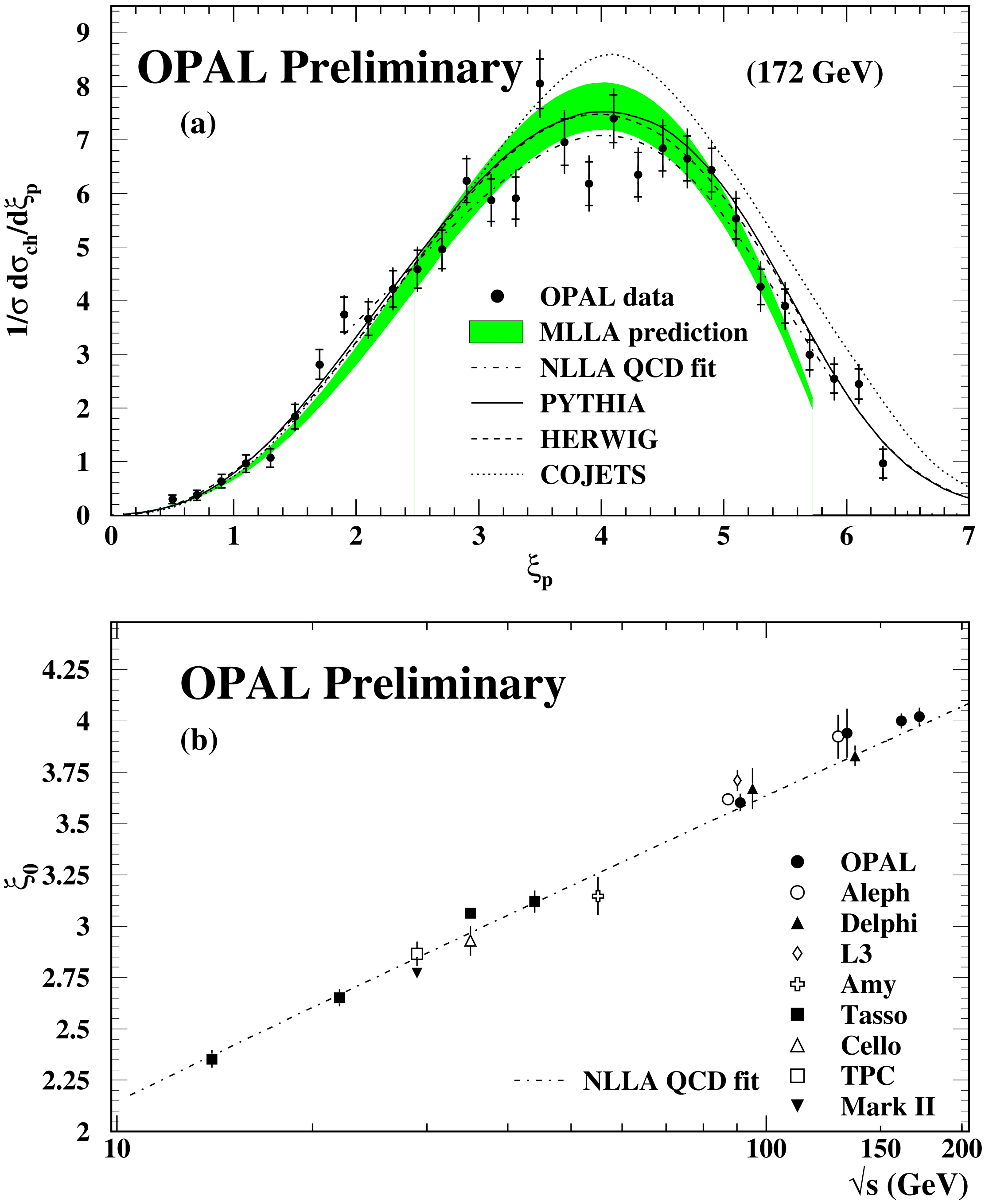

Figure 13: (a) Distribution of $\xi_p = \ln(1/x_p)$ for charged particles. Also shown are a fit of the NLLA QCD prediction, and predictions from MLLA QCD and PYTHIA, HERWIG and COJETS. The curve for the ARIADNE prediction is almost indistinguishable from the PYTHIA prediction and is omitted. (b) Evolution of the position of the peak of the ξ_p distribution, ξ_0, with the c.m. energy $\sqrt{s}$, compared with a fit of the NLLA QCD prediction up to and including the data at 161 GeV.

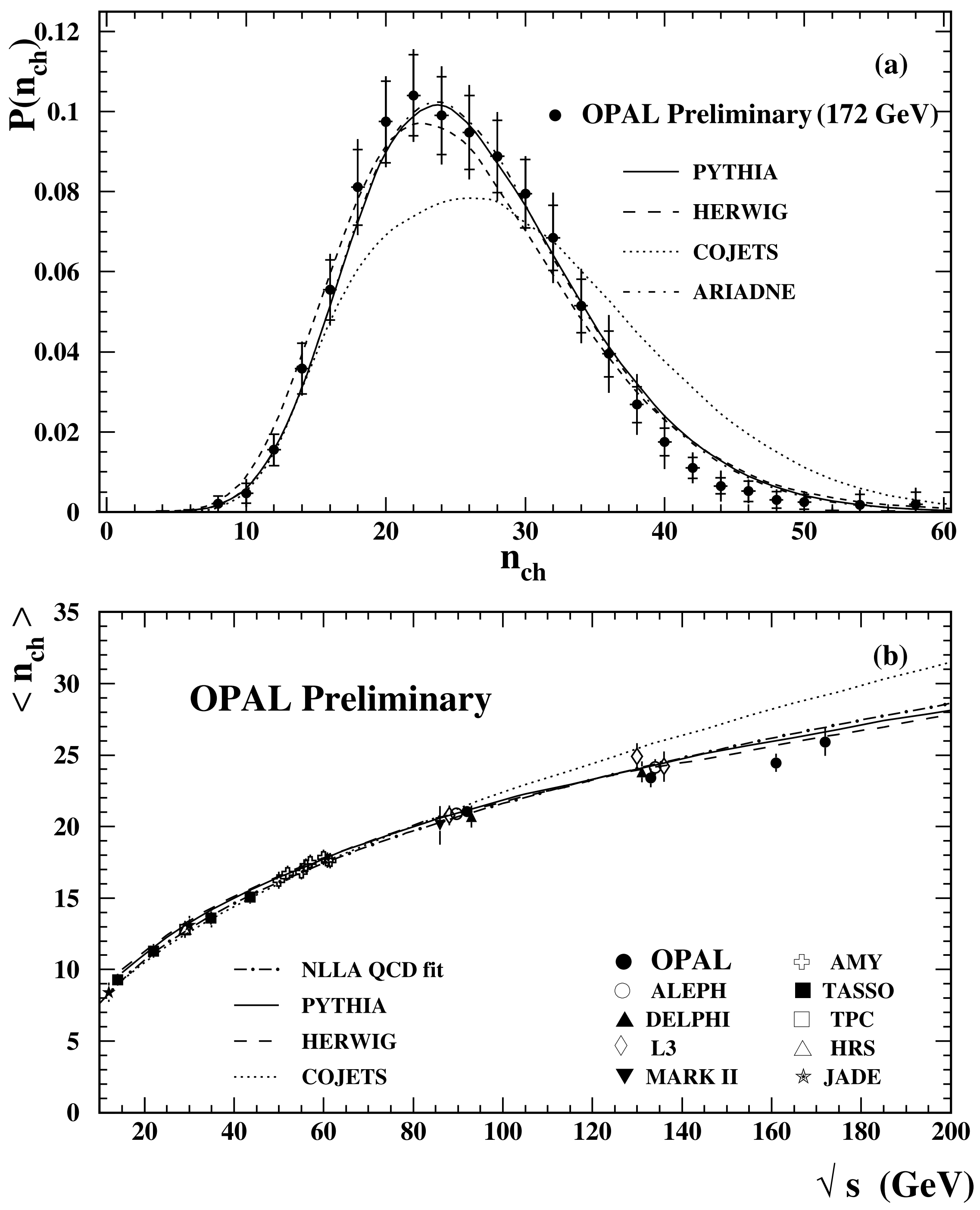

Figure 14: (a) Corrected distribution of the charged particle multiplicity $n_{\rm ch}$. Predictions from PYTHIA, HERWIG, COJETS and ARIADNE are also shown. (b) Mean charged particle multiplicity measurements over a range of $\sqrt{s}$ from 12 GeV to 172 GeV. The measurements are compared to a fit of the NLLA QCD prediction for the evolution of the charged particle multiplicity with $\sqrt{s}$, up to and including the data at 161 GeV, and to the predictions from PYTHIA, HERWIG, and COJETS. The curve for the ARIADNE prediction is almost indistinguishable from the PYTHIA prediction and is omitted.